

Southern Methodist University

SMU Scholar

Electrical Engineering Theses and Dissertations

Electrical Engineering

Spring 5-14-2022

The Transport of Acoustic Energy at Two-Dimensional Material Interfaces

Jesus Bolivar

Southern Methodist University, jesusb@smu.edu

Follow this and additional works at: https://scholar.smu.edu/engineering_electrical_etds



Part of the [Electrical and Computer Engineering Commons](#)

Recommended Citation

Bolivar, Jesus, "The Transport of Acoustic Energy at Two-Dimensional Material Interfaces" (2022).
Electrical Engineering Theses and Dissertations. 46.
https://scholar.smu.edu/engineering_electrical_etds/46

This Thesis is brought to you for free and open access by the Electrical Engineering at SMU Scholar. It has been accepted for inclusion in Electrical Engineering Theses and Dissertations by an authorized administrator of SMU Scholar. For more information, please visit <http://digitalrepository.smu.edu>.

THE TRANSPORT OF ACOUSTIC ENERGY AT TWO-DIMENSIONAL MATERIAL
INTERFACES

Approved by:

Kevin Brenner, Assistant Professor

J.-C. Chiao, Professor

Bruce Gnade, Clinical Professor

Prasanna Rangarajan, Assistant Professor

THE TRANSPORT OF ACOUSTIC ENERGY AT TWO-DIMENSIONAL MATERIAL
INTERFACES

A Thesis Presented to the Graduate Faculty of

Lyle School of Engineering

Southern Methodist University

in

Partial Fulfillment of the Requirements

for the degree of

Master of Science in Electrical Engineering

by

Jesus Alejandro Avendano Bolivar

B.S. in Mechatronics Engineering, Instituto Tecnológico de Saltillo

14 May 2022

ACKNOWLEDGEMENTS

I would like to acknowledge and give my gratitude to my advisor Dr. Kevin Brenner, whose knowledge, and support through all the steps of this project made its completion possible. For answering every question and for guiding me when I lacked knowledge or perspective to solve the problem at hand.

I would also like to acknowledge Dr. Bruce Gnade, Dr. Prasanna Rangarajan, and Dr. Jungchih Chiao, for reading my thesis and accepting being part of the committee. I appreciate them taking the time to contribute with their knowledge to make me a better researcher.

Additionally, I would like to thank Professor Michael Haberman, Mr. Sam Wallen and Mr. Sam Parker for performing the continuum modeling.

The Transport of Acoustic Energy at Two-Dimensional Material Interfaces

Advisor: Assistant Professor Kevin Brenner

Masters of Science conferred May 14, 2022

The control of vibrational energy within solids is a fundamental engineering challenge with numerous technological applications. While the control of electrons and photons has revolutionized computation and communication, the control of phonons, the quantized particle of vibrational energy, has been far less successful. Acoustic energy is a form of vibrational energy, but unlike heat, it involves coherent excitations of phonons to form larger elastic waves. It is this coherence that allows acoustic energy to be a valuable engineering tool for applications in imaging, timekeeping, and structural monitoring. As such, methods of isolating acoustic energy within solids are necessary to enable a wide range of technologies. Traditional methods of acoustic isolation involve interfacing different phases of matter to reflect via an impedance mismatch, like air gas and foams. The problem is that these methods are not scalable to extreme or nanoscale environments. It is not feasible to apply foams to hydrodynamic surfaces or within an integrated circuit. The objective of this proposal is to demonstrate methods of isolating acoustic energy by constructing solids with different types of chemical interactions, not by interfacing solids with different phases of matter. The impact of this is to enable technologies based on acoustic energy to access new applications that cannot be tapped with traditional isolation methods.

This thesis investigates the transport of acoustic energy at the interface of two-dimensional materials. Two-dimensional materials are crystalline layers of atoms that interface with other materials via a weak van der Waals interaction. Our investigation applies both computational and

experimental methods. The computational methods blend super-wavelength continuum models with sub-wavelength molecular dynamics simulations. Treating the interface as a thin plate coupled to a bulk elastic material by springs, we predict that the weak van der Waals interaction should produce a press-release boundary condition that reflects broad acoustic energy from infrasound to hypersound. The spring constant of the interface is verified with molecular dynamics simulations that extract a linear force-displacement relationship under an isothermal-isobaric ensemble, to mimic experimental conditions. These predictions are verified using pitch-catch experiments at 1 MHz in a water tank. The results of these experiments demonstrate nearly three-decibel attenuation from one graphene layer. When normalized to the atomic thickness of the graphene layer, this system provides orders of magnitude better isolation than foams, rubbers, or metasurfaces, in a manner that is scalable to extreme and nanoscale environments.

TABLE OF CONTENTS

LIST OF FIGURES	vii
Chapter	
I. INTRODUCTION	1
II. THEORETICAL INVESTIGATION OF ACOUSTIC TRANSPORT	5
III. EXPERIMENTAL INVESTIGATION OF ACOUSTIC TRANSPORT	16
IV. CONCLUSIONS AND FUTURE WORK	25
REFERENCES	28

LIST OF FIGURES

Figure	Page
1. Continuum and atomistic views of the 2D material interface	5
2. Solving an impedance analogy for two graphene layer interfaces.	6
3. MD simulations to minimize and equilibrate the graphene layer	9
4. MD simulations to minimize and equilibrate the substrate	11
5. MD simulations to minimize and equilibrate the graphene layer on the substrate	13
6. MD simulations to extract a spring constant associated with the interface	14
7. Standing waves formed in catch signal with short cylinder	17
8. The transfer process used to form test samples	18
9. Raman spectra of transferred monolayer graphene on our cylinder	19
10. Pitch-catch setup for experimental testing	20
11. Pitch-catch experiments on a cylinder with a monolayer of graphene	21
12. Pitch-catch experiments on a cylinder with graphene ink	22
13. Pitch-catch experiments on a cylinder with one and two graphene layers	23
14. Concept of acoustic guiding within a solid fiber	25
15. Illustration of wave motion modifying interlayer phenomena in vdW heterostructures	26

DEDICATIONS

Every challenging work needs discipline and self-effort as well as support and guidance from those who are very close to our hearts.

This Thesis is dedicated to my mother and siblings, whose affection, love, and encouragement have backed me up every day and motivated me to keep going forward. The completion of this would not have been possible without them.

Additionally, I would like to dedicate it to my friends and peers, whose support has been with me since the moment they knew I started this journey and are with me until this day.

Chapter 1

INTRODUCTION

Controlling energy is central to almost every aspect of Electrical and Computer Engineering (ECE). This includes controlling the way that energy propagates within solids. Historically, we have had tremendous success controlling how electrons (charge) and photons (light) propagate in solids. This has led to technologies such as integrated circuits and optical waveguides that have revolutionized the way that we compute and communicate. We have had far less success controlling phonons (heat and sound), which are the quantized particles of vibrational energy. In fact, phonons are often viewed as a form of energy that we must manage, rather than use. For example, packaging for heat dissipation or earplugs for sound isolation. The difficulty in controlling phonons in solids arises from a handful of reasons. One reason is that phonons cannot be electrostatically controlled as electrons can be. Another reason is that solids simply have a much larger range of electrical resistivities than vibrational resistivities. Electrical resistivities span twenty-four orders of magnitude (quartz to Ag¹), while thermal conductivities barely span six orders of magnitude (polymers to diamond²⁻³). Finally, when the phonon transport at a solid-solid interface is acoustic versus diffusive, the reflection probability is based on the density (ρ) mismatch between the two solids⁴. As such, reflections between solids are weak, as they all share comparable densities.

Today, methods of isolating phonons generally involve three approaches. The first approach is to create disorder to hinder the phonon propagation. For example, previous records for thermal resistivity in solids involved highly defective materials⁵. This is also the reason that the thermal conductivity of nanowires is much lower than bulk forms, due to phonon scattering at the

Surface⁶. The second approach is to create metamaterials or metasurfaces, which are micro or nano-fabricated structures that artificially create forbidden ranges of phonon frequencies^{7,8}. For example, phononic crystals. The third approach is to interface solids with different phases of matter. For example, the air gaps or foams that are found in most heat and sound isolation technologies. While the first two approaches are valuable for attenuating hot or loud spots, it is only the third method that is viable for reflecting this energy. Reflection being the foundation for waveguides. For example, a desirable technology is a vibrational equivalent to an optical fiber that could transport acoustic energy over long distances for applications in structural monitoring. Here, an acoustic cladding layer is needed that reflects energy back into the fiber, rather than allowing it to leak into the environment and be attenuated. To date, no such acoustic cladding exists in the solid-state.

Acoustic energy is essentially a coherent excitation of phonons to form a larger elastic wave⁹. It is similar to thermal energy, but heat involves phonons of much higher frequency, density, and lacking coherence. It is this coherence that allows acoustic energy to be a valuable engineering tool for applications like imaging¹⁰, time keeping¹¹, and structural monitoring. Acoustic energy can range in frequency from infrasound (Hz range) to hypersound (GHz range), with ultrasound (MHz range) being the most commonly used for engineering applications. For example, ultrasound is the workhorse of medical imaging. Acoustic energy is generally excited by transducers using one of two methods. The most common is a piezoelectric transducer, which uses the piezoelectric effect that couples pressure and voltage in a crystalline material. The second method is a membrane transducer, which is typically called a capacitive micromachined ultrasonic transducer (CMUT)¹². Here, a membrane is electrostatically deflected to produce surface pressures at the desired frequency.

The definition of acoustic energy is also different from thermal energy. Thermal energy (E_T) is simply the kinetic energy of all the atomic vibrations in a solid, which is then scaled by the

Boltzmann constant (k_B) to give temperature (T). Acoustic energy (E_A) is the sum of the kinetic energy from the atomic vibrations and the potential energy from the atomic displacement. In a volume of material, we would define

$$E_A = \frac{1}{2}TS + \frac{1}{2}\rho v^2 \quad \text{Equation 1}$$

where T is the stress, S is the strain, ρ is the mass density, and v is the atomic velocity¹⁰. Because of this definition, pressure continuity across an interface must be maintained as part of energy conservation. This gives rise to the concept of a pressure-release boundary condition (PRBC).

When acoustic energy is propagating in a material with a larger acoustic impedance (Z), and then meets a material with a significantly lower Z , there is a loss of pressure across the interfaces which causes the acoustic energy to be reflected back. This can be quantified through the reflection coefficient (Γ) between two materials

$$\Gamma = \frac{Z_2 - Z_1}{Z_2 + Z_1} \quad \text{Equation 2}$$

where Z_1 and Z_2 are the acoustic impedances of the two materials¹⁰. As Z is a function of the density and sound velocity (strength of chemical bonds) in a material, it is similar among solids and thus hard to reflect acoustic energy between solids. To date, there have been scant reports of a PRBC with solid-like materials.

The problem that this thesis addresses is that current sound isolation methods are not scalable to extreme or nanoscale environments. It is not feasible to apply foams to hydrodynamic surfaces or within integrated circuits (ICs). This also holds true for acoustic metamaterials that involve complex nano-scale fabrication^{7,8}. As such, engineering applications that make use of acoustic energy are limited. The objective of this thesis is to demonstrate control of ultrasound within solids by constructing materials based on mismatched chemical bonding, rather than mismatched phases of matter. Specifically, this thesis investigates the propagation of acoustic energy at the interfaces of two-dimensional (2D) materials¹³. The extremely weak chemical interaction

between 2D materials and other bulk materials can create a PRBC between solids¹¹, reflecting significant amounts of acoustic energy in a material system that is only a few atoms thick.

Chapter 2

THEORETICAL INVESTIGATION OF ACOUSTIC TRANSPORT

The theoretical methods that we applied viewed the interface as both super-wavelength (continuum) and sub-wavelength (atomistic) systems, **Figure 1**. The continuum models treat the supported 2D material as a thin plate coupled to a bulk elastic material with springs. A similar model has been applied to successfully describe thermal transport at 2D-bulk interfaces¹⁵⁻¹⁷. The spring constant coupling the two materials is derived from the vdW interaction. This vdW interaction is modeled with a 6-12 Lennard-Jones (LJ) potential¹⁸. The vdW interaction is highly dependent upon a number of physical properties of the interface, such as crystallographic rotation¹⁶, chemical disorder²⁰, and temperature¹⁸. As such, it is necessary to verify this spring constant with molecular dynamics simulations (described later), as opposed to simply assigning a spring constant directly from the potential.

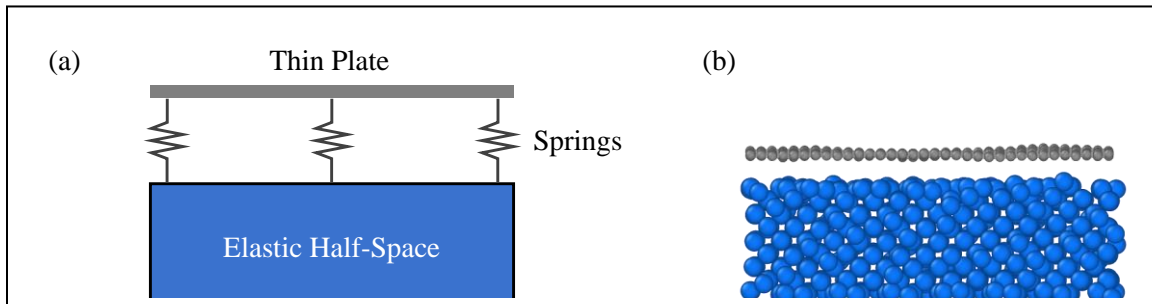


Figure 1. Continuum and atomistic views of the 2D material interface. (a) The continuum view is a thin plate coupled to an elastic half-space with springs. (b) The atomistic view is atoms bounded by many-body (intra-material) and LJ (inter-materials) potentials.

Adopting this continuum view, we begin to investigate the acoustic transport at normal incidence. To do this, we develop an equivalent based on an impedance analogy. The transmission at normal incidence can then be solved based on the elastic properties of the materials and interface, **Figure 2**. A two-layer graphene system is used to ensure that there is a definitive solid-solid vdW interaction. The impedance associated with the interface is found to be roughly 1×10^5 Rayl, assuming the 1 cm^2 sample used in our experiments and a spring constant of 5.1 N/m . This spring constant is derived directly from the LJ potential and verified with MD in the below section. The impedance is highly mismatched with fluids or metals, which are nearly an order of magnitude larger at 1×10^6 and 3.3×10^7 Rayl, respectively. This mismatch in impedance is expected to reflect acoustic energy in the ultrasound range ($0.01 - 1 \text{ MHz}$). In addition to this, there are tunable resonances that exist based on the area of the graphene sheet, which may be valuable for a variety of technologies.

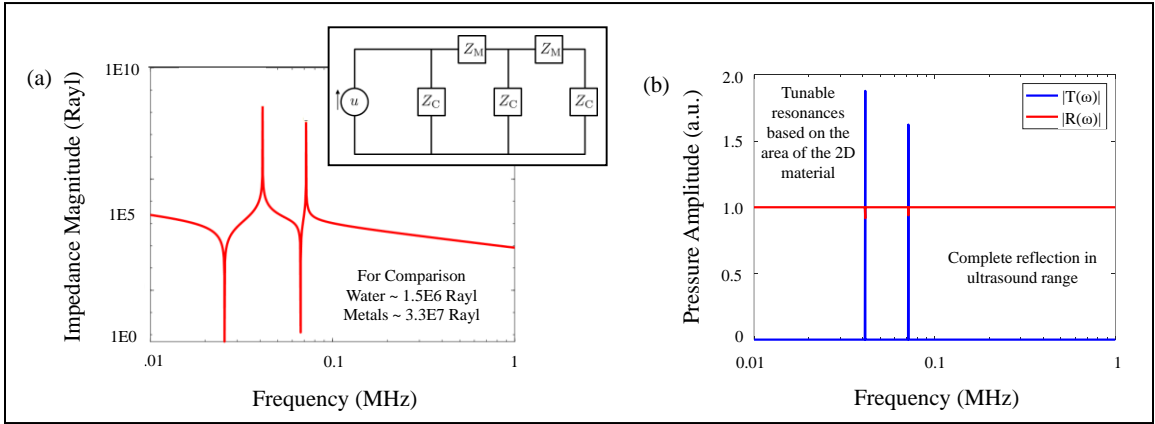


Figure 2. Solving an impedance analogy for the two-graphene layer interface. (a) The impedance of the interface in the ultrasound range. Tunable resonances are observed based on the area of the graphene layer. Inset shows the equivalent circuit used for the calculation. Z_M is related to the graphene layer while Z_C is related to the vdW interaction. (b) The reflection and transmission coefficients indicate strong reflections in the ultrasound range.

MD simulations are used to verify the spring constant associated with the interface, which is one of the larger assumptions being made in the continuum model. These simulations essentially solve Newton's equations of motion for a system of atoms bound by interatomic potentials. As such, they capture information, like many-body and anharmonic effects, that are not captured in the continuum models. These simulations are implemented in LAMMPS, which is a highly parallelized software for solving these equations²². All simulations are run on Southern Methodist University's (SMU's) ManeFrame II HPC using Nvidia P100 GPUs, and are run for 200 ps with timesteps of 0.01 fs. System data on temperature and pressure is sampled every 10 fs. Temperature is calculated as the kinetic energy of all atoms scaled by the Boltzmann constant. Pressure is calculated as

$$P = \frac{Nk_B T}{V} + \frac{\sum r \cdot f}{dV} \quad \text{Equation 3}$$

where N is the number of atoms in the system, V is the volume, d is the dimensionality of the system, r is the position of an atom, and f is the force of an atom.

All simulations apply periodic boundary conditions in the x and y directions. In the z-direction, a fixed boundary condition is used with a vacuum layer between the atoms and the boundary so that the atoms can freely displace and reconstruct. The first step in this simulation is to independently equilibrate the graphene and bulk materials. A monolayer system consisting of 680 atoms is formed to match the lattice constant and density of graphene, and carbon atoms are bound by a many-body potential. Specifically, a Tersoff potential that has been optimized for the vibrational properties of graphene²³. The system is then minimized until the potential energy between atoms is less than 1×10^{-10} Kcal/mol and the force between atoms is less than 1×10^{-10} Kcal/mol-Å. The system is then equilibrated using an isothermal-isobaric ensemble at 293 K and 1 atm, **Figure 3**. This is also referred to as an NPT ensemble as it conserves energy by maintaining a constant number of atoms, pressure, and temperature. Thermostating is done with a Nose-Hoover thermostat that introduces an extra degree of freedom to the Hamiltonian to

couple the system to a heat bath²⁴. Barostating is done by modifying the simulation size at each timestep in order to regulate the pressure. As such, we only apply a barostat to the x and y-directions that have periodic boundary conditions.

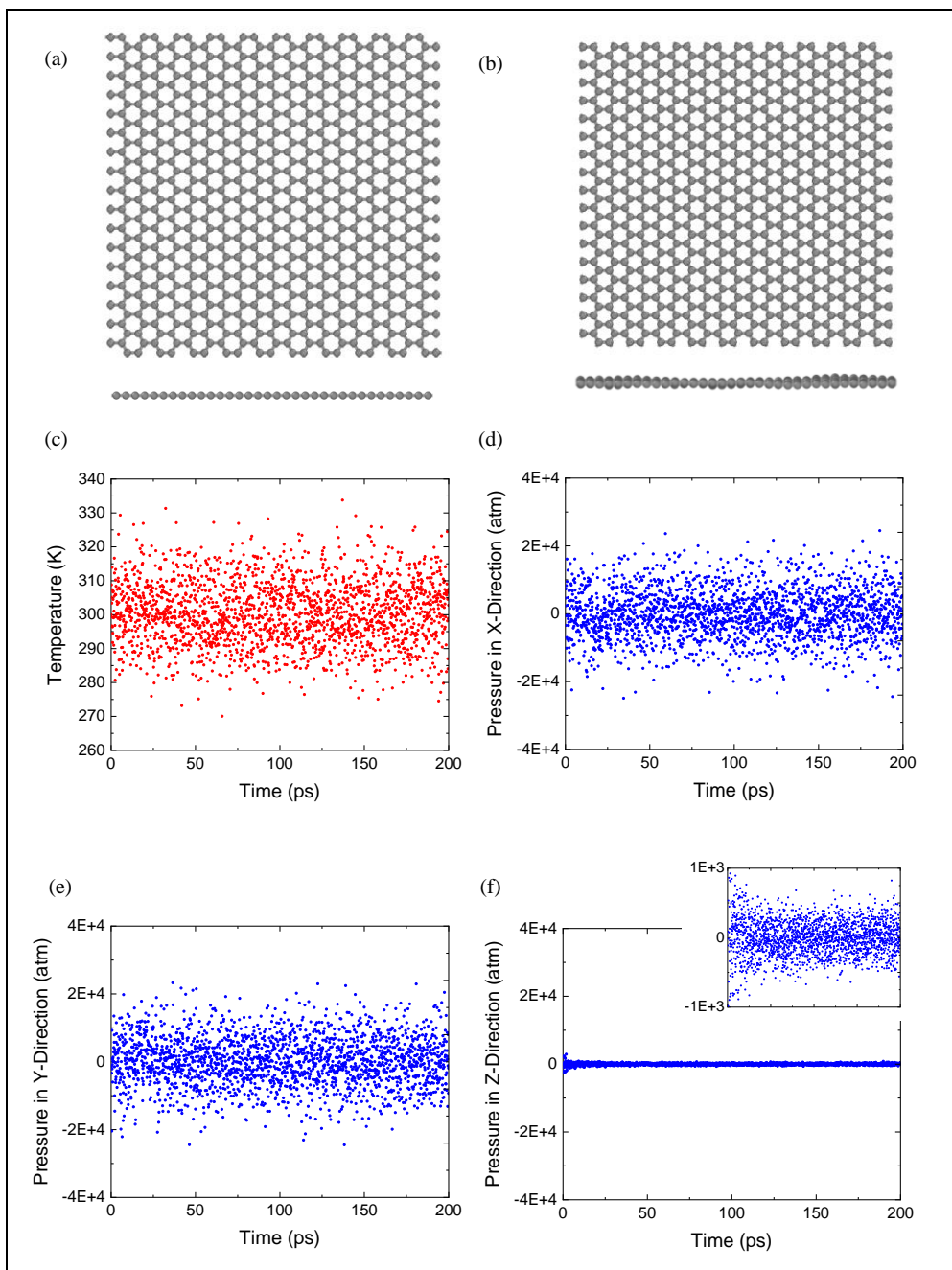


Figure 3. MD simulations to minimize and equilibrate the graphene layer. (a) Graphene layer matched to lattice constant and density. (b) Graphene layer minimized and equilibrated. (c) System temperature. (d) System pressure in x-direction. (e) System pressure in the y-direction. (f) System pressure in the z-direction. Inset shows zoomed-in view.

Next, the substrate is equilibrated. A multilayer system consisting of 1080 atoms is formed to match the lattice constant and density of Si, and Si atoms are bound by a many-body potential. Specifically, a Tersoff potential that has been optimized for the vibrational properties of Si²⁵. The bottom layer of Si atoms is then frozen (their force set to zero) to anchor the system. The system is then minimized until the potential energy between atoms is less than 1×10^{-10} Kcal/mol and the force between atoms is less than 1×10^{-10} Kcal/mol-. The system is then equilibrated using an isothermal isobaric ensemble at 293 K and 1 atm, **Figure 4**.

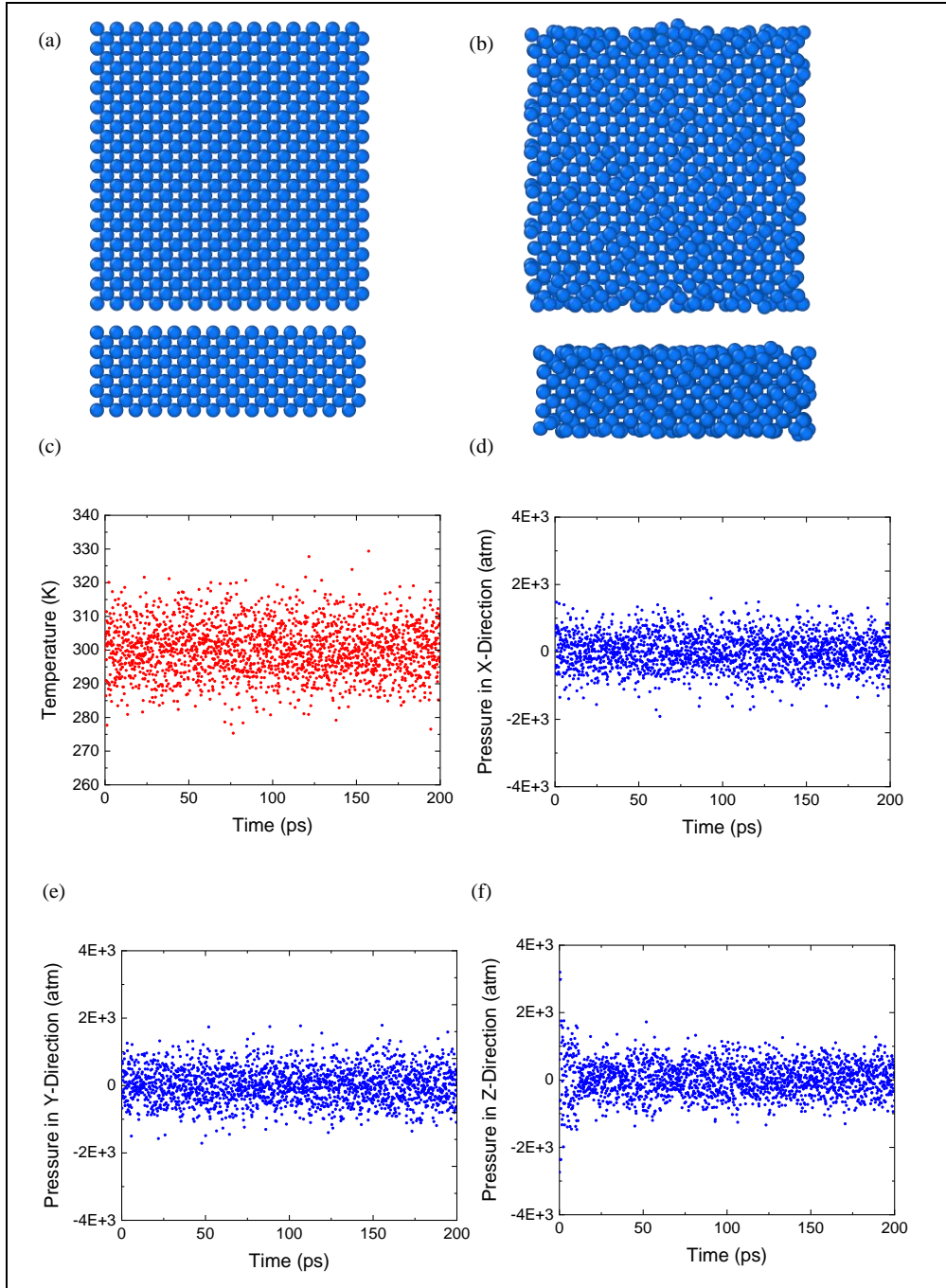


Figure 4. MD simulations to minimize and equilibrate the substrate. (a) A few layers matched to lattice constant and density of Si. (b) Si layer minimized and equilibrated. (c) System temperature. (d) System pressure in x-direction. (e) System pressure in y-direction. (f) System pressure in z-direction.

Finally, the equilibrated graphene layer and substrate are brought together and equilibrated as a system. The atomic positions and velocities from the final timestep of the previous equilibrations are saved. A pairwise potential is used that applies a 6-12 Lennard-Jones potential between the Si and carbon atoms, while maintaining the same Tersoff potentials within the materials. The graphene layer is then placed at the minimum energy distance of 3.629 Å from the surface of the Si. The system is then minimized until the potential energy between atoms is less than 2×10^{-5} Kcal/mol and the force between atoms is less than 2×10^{-1} Kcal/mol-Å. The system is then equilibrated using an isothermal isobaric ensemble at 293 K and 1 atm, **Figure 5**.

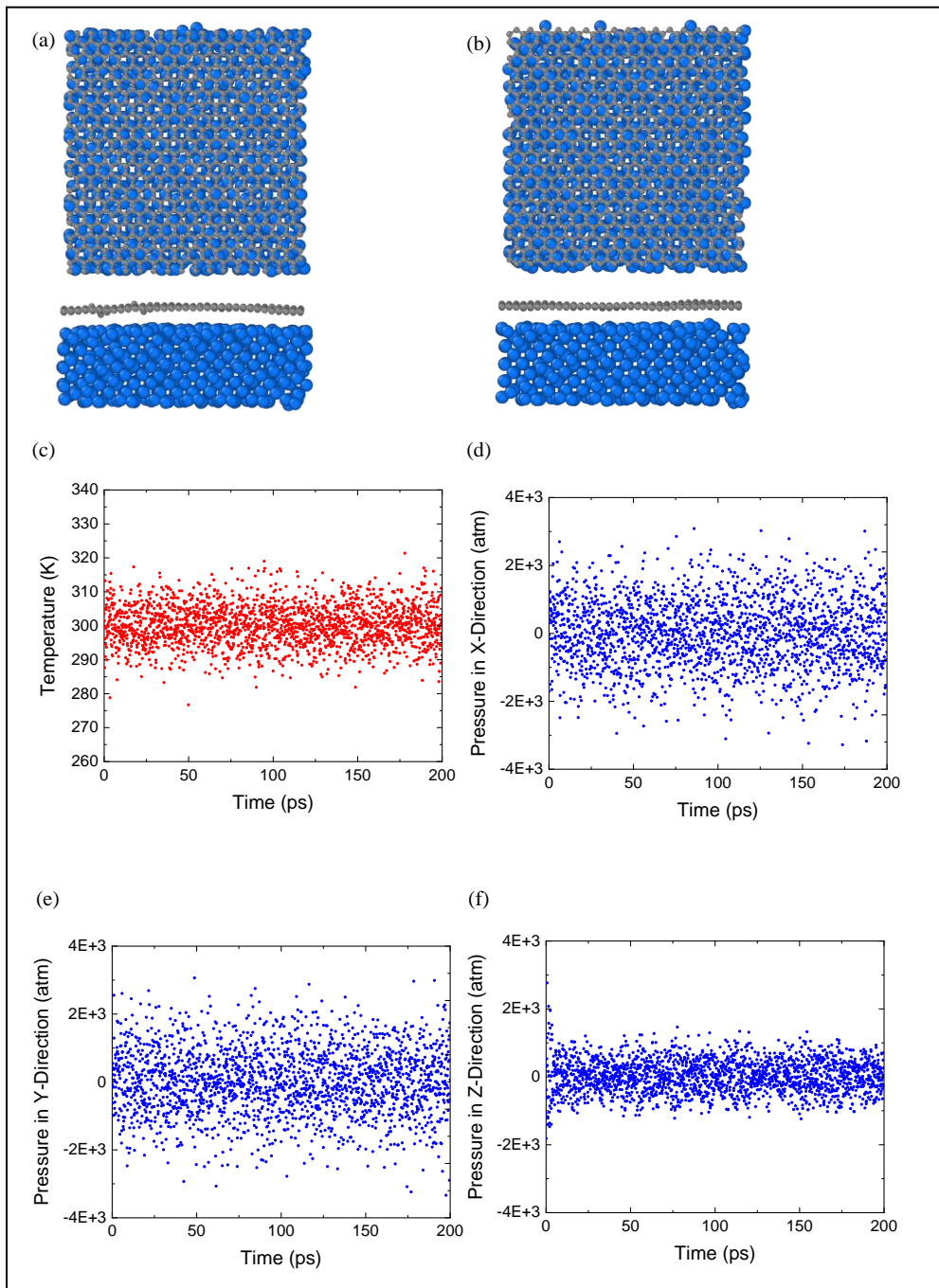


Figure 5. MD simulations to minimize and equilibrate the interface. (a) The equilibrated graphene layer is placed on the equilibrated substrate to form the interface. (b) The system is minimized and equilibrated. (c) System temperature. (d) System pressure in the x-direction. (e) System pressure in the y-direction. (f) System pressure in the z-direction.

Once the graphene and substrate system is equilibrated, the spring constant of the interface is extracted. We extracted this value by applying a force to all atoms in the graphene layer in the negative z-direction. This force is superimposed upon forces from the thermostat and barostat, so it is run simultaneously with the isothermal-isobaric ensemble at 293 K and 1 atm (in the x and y-directions). The bottom atoms in the substrate remain frozen to anchor the system so that the interface is pressurized without creating a uniform displacement of the system. The averaged displacement over the 200 ps simulation is then plotted as a function of the force to extract a force constant for the interface, **Figure 6**.

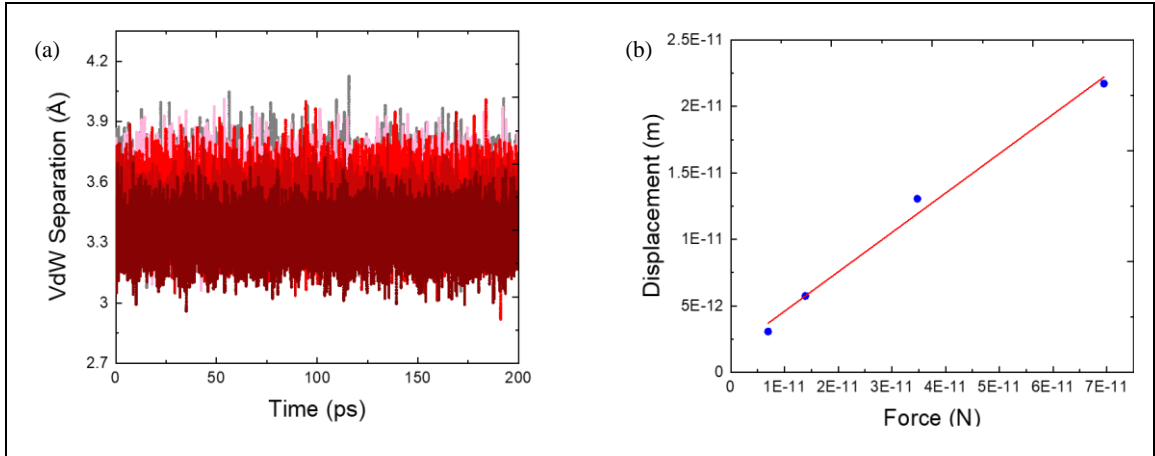


Figure 6. MD simulations to extract a spring constant associated with the interface. (a) The vdW separation at various forces is applied to the graphene layer. The layers are 0 N (black), 6.9×10^{-12} N (pink), 1.4×10^{-11} N (red), 3.5×10^{-11} N (dark red), 6.9×10^{-11} N (very dark red). (b) The displacement versus force for the pressurized interface.

These simulations extract a force constant of ~ 3.34 N/m. This value is comparable to the spring constant derived directly from the LJ potential, and supports the theory that a PRBC should exist. The discrepancies between these two values could arise from a number of reasons. The first is related to the statistical averaging, which may require longer simulations or smaller time resolutions. The second could be that the cutoff distance for the LJ potential is set at 10 \AA , so the graphene layer is feeling the interaction of multiple layers of substrate atoms as opposed to simply connecting a spring to the top layer of atoms.

Chapter 3

EXPERIMENTAL INVESTIGATION OF THE ACOUSTIC TRANSPORT

The experimental methods we applied involved a pitch-catch set up in a water tank. Samples are fabricated by transferring monolayer graphene onto a custom-fabricated quartz cylinder with a surface roughness of below 1 nm. The diameter of the quartz cylinder was 50 mm and the length is 75 mm. The diameter was selected to be larger than the diameter of our transducers (13 mm). The length is selected based on both the spatial wavelength of the ultrasound, and the temporal length of the ultrasound burst from the transducer. If the cylinder's length is below the wavelength, the ultrasound will result in a uniform displacement of the cylinder as opposed to the coupling of the wave into the cylinder. Also, if the cylinder's length is too short, the ultrasound will propagate through the cylinder and reflect back to superimpose on the burst that is still entering the cylinder. If these criteria are not met, standing waves can form and disrupt the measurement, **Figure 7**. In **Figure 7a**, clear bursts are not visible due to overlapping of the entering and existing burst. In **Figure 7b**, there are large losses of acoustic energy near the center frequency of the transducer, which we speculate to be from the formation of standing waves in the short cylinder.

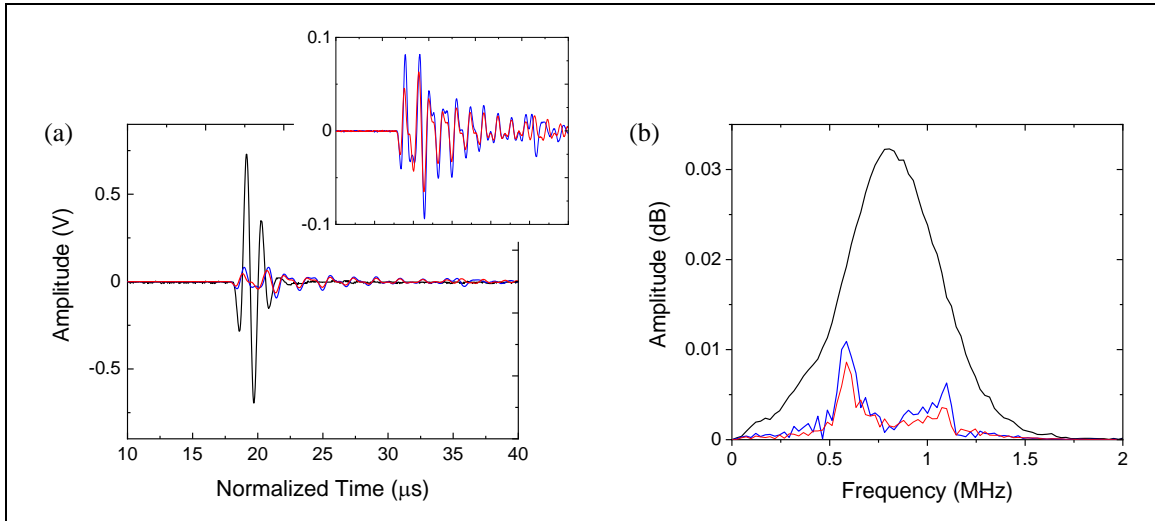


Figure 7. Standing waves formed in catch signal with a short cylinder. (a) The entering burst overlaps with the reflecting burst. (b) Gaps in the catch signal bandwidth are suspected to be from standing waves.

Monolayer graphene was grown using chemical vapor deposition (CVD) on Cu foils²⁶. The graphene was transferred onto one face of the cylinder using a wet transfer process²⁷, **Figure 8**. In this process, the graphene-Cu foil is coated with 500 nm layer of poly(methyl methacrylate) (PMMA) via spin coating. The PMMA-graphene-Cu foil is then placed in a solution of 1M FeCl₃ to chemically etch the underlying Cu layer. The PMMA-graphene layer is then collected on a glass slide and placed into a deionized (DI) water bath to remove the etchant. This is repeated with two other DI water baths, and then the sample is collected on the face of the cylinder. The cylinder is then heated to the glass transition temperature of the PMMA (100°C for 15 minutes) to form an intimate adhesion between the 2D material and the cylinder. The cylinder is then placed in acetone for 24 hours to remove the polymer layer.

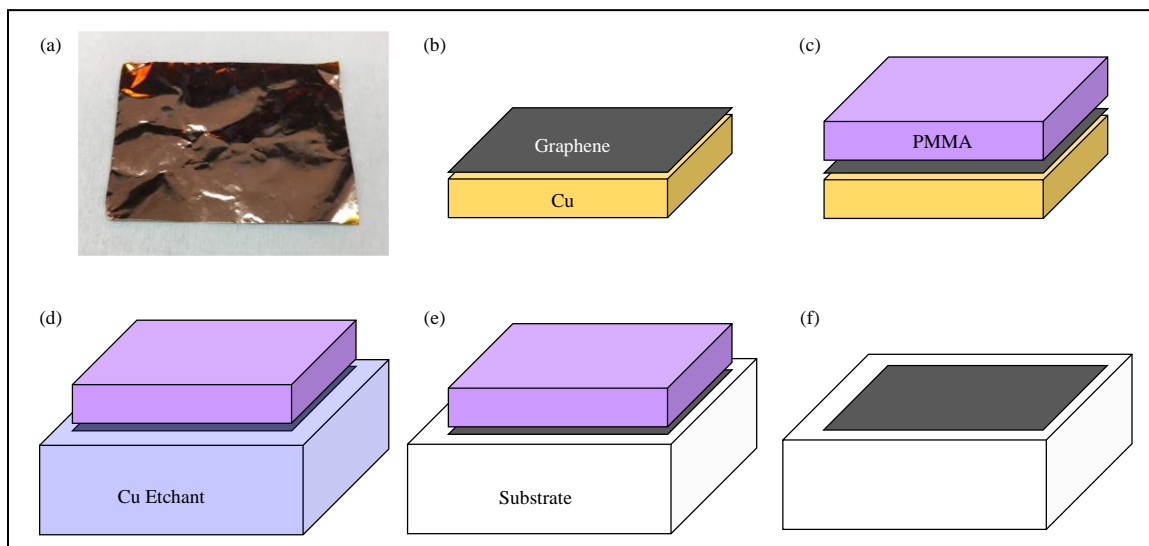


Figure 8. The transfer process used to form test samples. (a) Monolayer graphene is grown on Cu foil. (b) The starting point of the transfer process is monolayer graphene on Cu foil. (c) The supporting layer of PMMA is spin-coated. (d) The Cu is etched in solution. (e) The graphene with PMMA is collected on the substrate. (f) The PMMA is softened and removed with a 24-hour soak in acetone.

Raman spectroscopy is then performed to verify the presence and quality of the graphene layer, **Figure 9**. Raman is a powerful and non-destructive means of determining the number of layers and quality of graphene and graphite²⁸. The number of graphene layers can be determined by the number of the position and linewidth of the G and 2D peaks at 1580 cm^{-1} and $2,700\text{ cm}^{-1}$, respectively²⁸. The general quality of the material can be determined by the presence (or lack) of a defect-enabled peak called the D-peak at $\sim 1,350\text{ cm}^{-1}$. The Raman of our graphene layer, after transfer, indicates a high-quality monolayer²⁶.

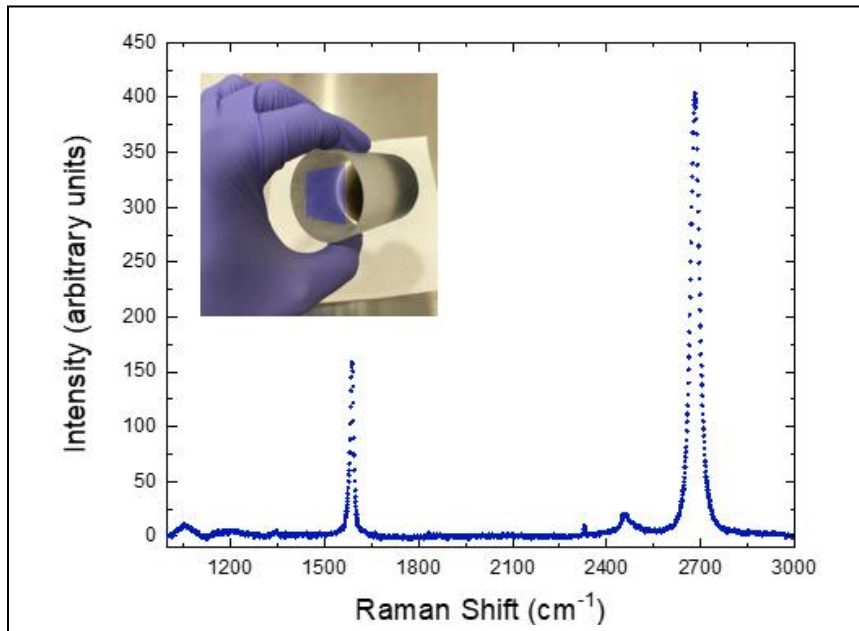


Figure 9. Raman spectra of transferred monolayer graphene on our cylinder. The lack of a D-peak at $1,350\text{ cm}^{-1}$ indicates high-quality material. Inset shows the cylinder with graphene layer highlighted.

The propagation of normally-incident ultrasound is investigated using a pitch-catch setup in a water tank, **Figure 10**. A pitch-catch setup uses two transducers, one to excite the signal and one to receive it on the back (transmitted) side of the cylinder. Two piezoelectric immersion transducers (Olympus V303-SU) with a 1 MHz center frequency and a 13 mm diameter face are fixed with clamps in a water tank. The water tank is supported on a vibration-isolation (nitrogen-floated) table to limit external disturbances. The substrate is then placed between the two transducers. The pitch transducer is excited with a -50 V spike excitation that has a $1\ \mu\text{s}$ pulse width, which produces an approximately $4\ \mu\text{s}$ burst. The burst is set with a function generator (Keysight 33612A) that is run into a power amplifier (Minicircuits LZY-22+). The catch

transducer then receives the transmitted ultrasound, which is fed into an oscilloscope (Keysight DSOX3024T). The oscilloscope captures the waveform in the time domain and in the frequency domain by performing Fourier analysis. All experiments capture three conditions. The first condition is the blank water bath with no cylinder, which reveals details on the output pressure of the transducer over its bandwidth, along with the spacing of the transducers based on the sound velocity in water. The second condition is a bare cylinder with no coating on the surface. These functions are our baseline to compare against the coated cylinder. The third condition is the same cylinder coated with the 2D material(s). Extreme care is taken to ensure that no other aspects of the experimental setup change between all three conditions.

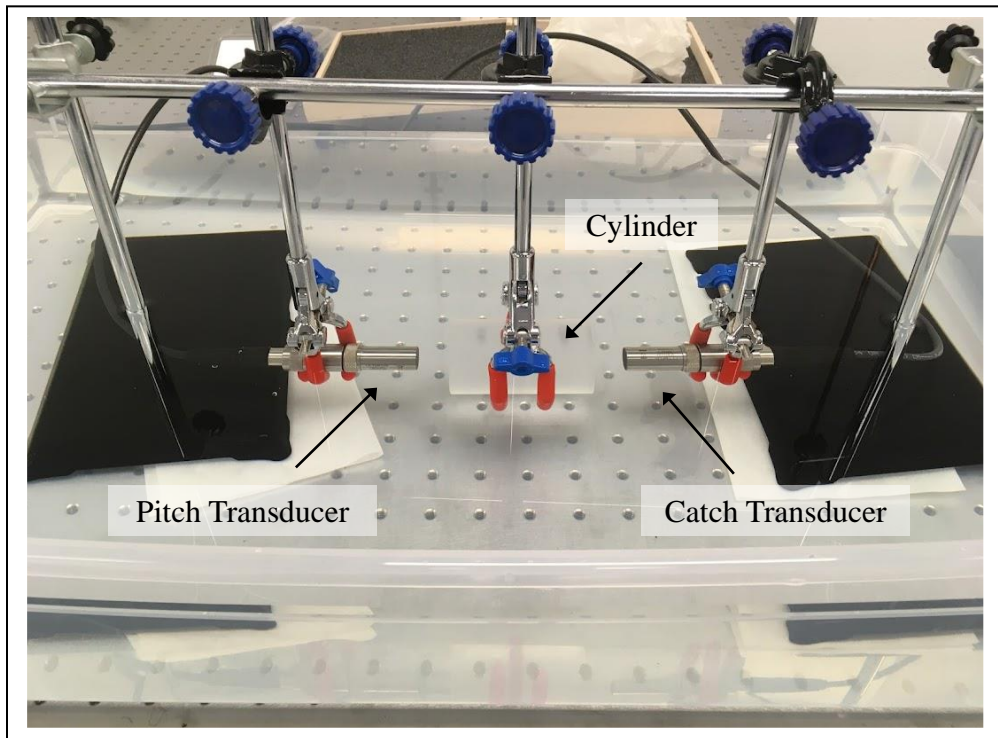


Figure 10. Pitch-catch setup for experimental testing. The pitch and catch transducers, along with the cylinder are annotated.

The first set of experiments tested cylinders with a monolayer of graphene, **Figure 11**. A single waveform, normalized in the time domain is shown along with the frequency analysis of an

average of 10 experiments. A roughly 3 dB attenuation in acoustic pressure is consistently seen among multiple samples. For all experiments, extreme care is taken to ensure that the surface is free of other residues from processing that may contribute to the reflection. A bare cylinder was also polymerized and soaked to verify there was minimal change when going through the graphene transfer process.

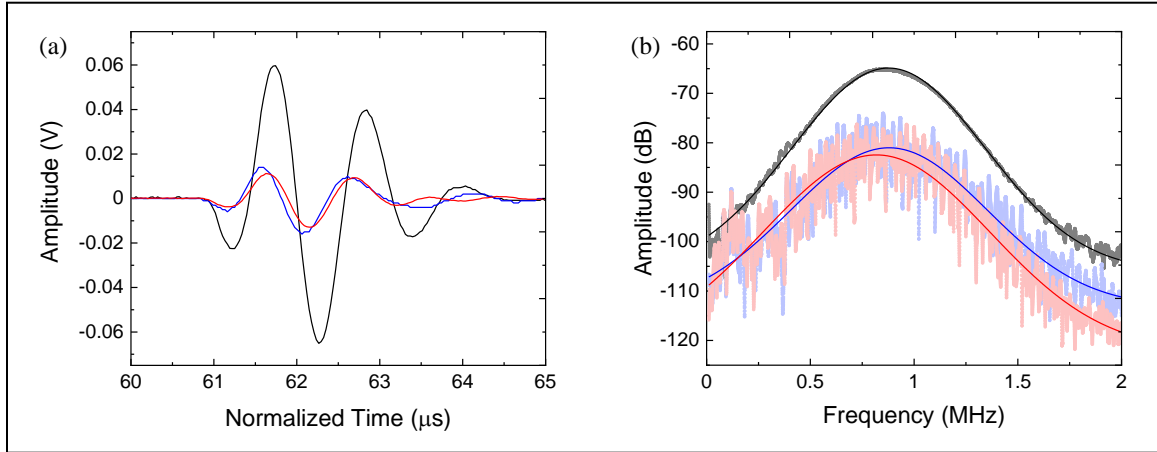


Figure 11. Pitch-catch experiments on a cylinder with a monolayer of graphene. (a) The waveform for the empty tank (black), bare cylinder (blue), and coated cylinder (red). (b) The frequency analysis for the empty tank (black), bare cylinder (blue), and coated cylinder (red). The data is an average of ten experiments.

The next set of experiments tested cylinders with a thin layer of graphene ink applied, **Figure 12**. The purpose of this experiment was to explore more scalable and commercial methods of applying graphene to arbitrary surfaces. A single waveform, normalized in the time domain is shown along with the frequency analysis of an average of 10 experiments. A roughly 5 dB attenuation in acoustic pressure is consistently seen among multiple samples.

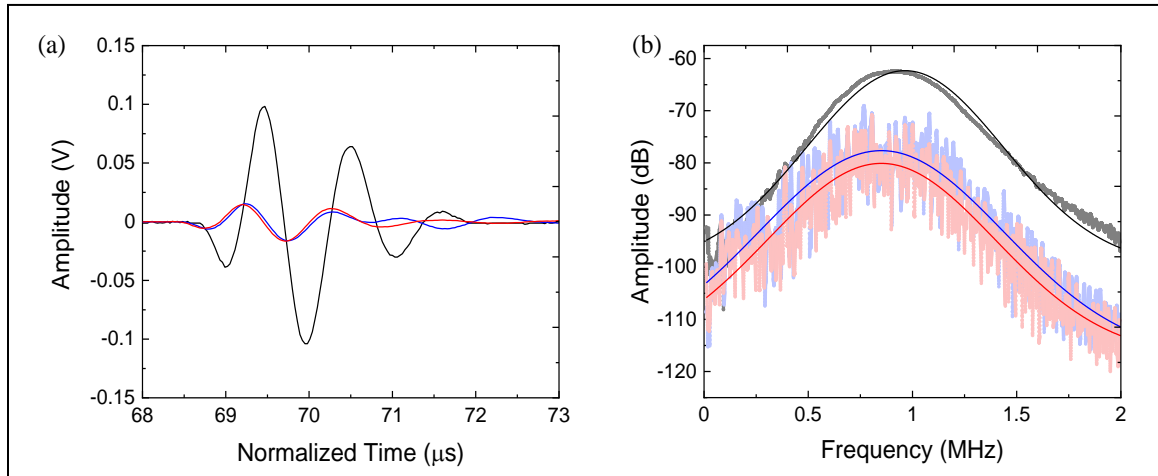


Figure 12. Pitch-catch experiments on a cylinder with graphene ink. (a) The wave form for the empty tank (black), bare cylinder (blue), and coated cylinder (red). (b) The frequency analysis for the empty tank (black), bare cylinder (blue), and coated cylinder (red). The data is an average of ten experiments.

An important property of this method is its scalability with the number of graphene layers (or the number of vdW interfaces the acoustic energy must cross). As such, we compared experiments with one and two graphene layers, whereby the second graphene layer was applied by simply repeating the transfer process, **Figure 13**. Although this experiment was run on a shorter substrate, which affected the frequency analysis, the waveforms clearly show increased reflections with the addition of a second graphene layer. Further exploring this scalability is a central component of our future work.

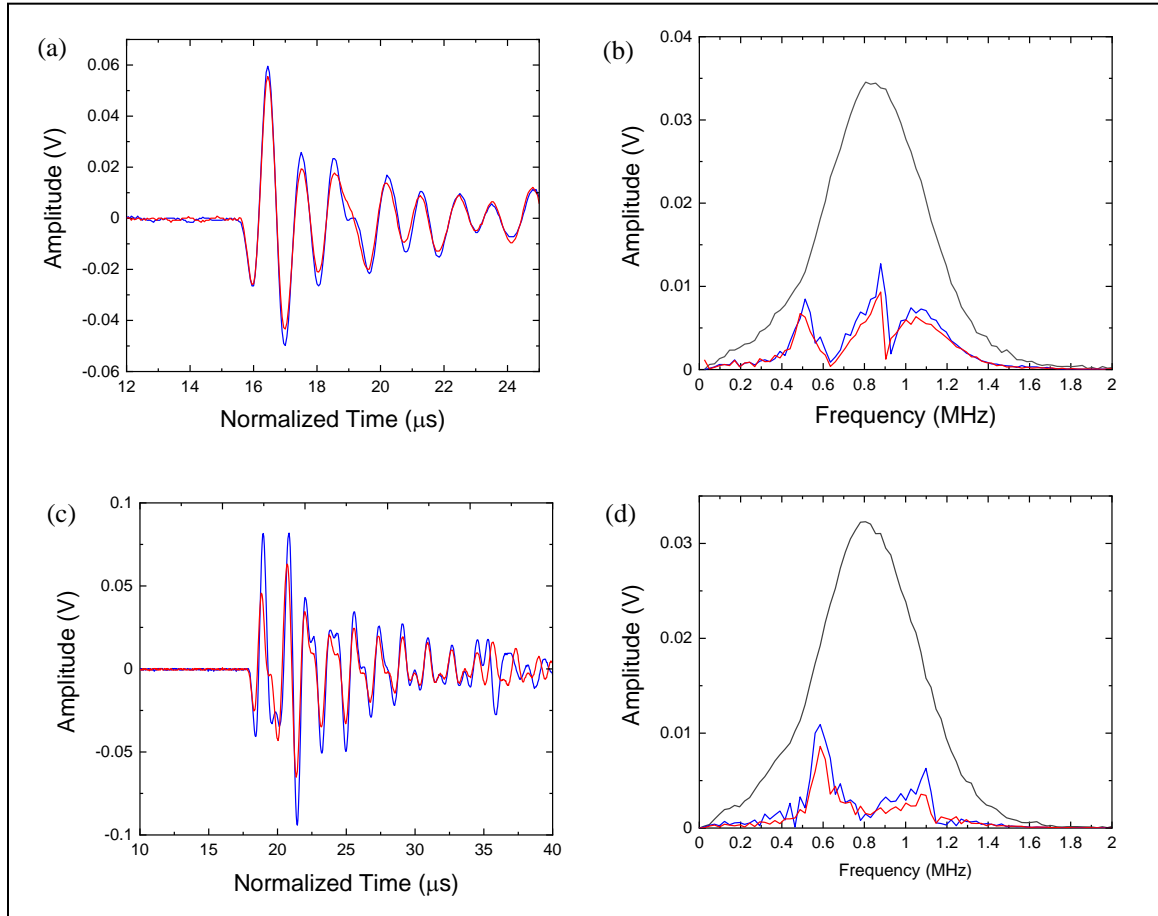


Figure 13. Pitch-catch experiments on a cylinder with one and two graphene layers. (a) The waveform for the bare cylinder (blue), and cylinder coated with one graphene layer (red). (b) The frequency analysis for the Pitch-Catch with no cylinder (black), the same bare cylinder (blue), cylinder coated with one graphene layer (red). (c), and the waveform for the bare cylinder (blue), and cylinder coated with two graphene layers (red). (d) The frequency analysis for the Pitch-Catch with no cylinder (black), same bare cylinder (blue), and cylinder coated with two graphene layers (red).

In general, when averaging multiple acquisitions off multiple experiments, an approximate -3 dB attenuation is seen from a single graphene layer. While this value is less than the complete reflection predicted from our theoretical work, it is still a record value. When normalizing this attenuation to the atomic thickness of the interface (and extrapolating to a bulk material), it provides orders of magnitude better attenuation than air gaps, foams, or polymers. Moreover, it is

scalable to both harsh and nano-scale environments due to the high melting point, low volume, and CMOS-compatibility of graphene.

CONCLUSIONS AND FUTURE WORK

Our future work has three objectives. The first is to extend the theory and experiments to an acoustic equivalent of an optical fiber, **Figure 14**. The concept here is that these PRBCs from the vdW interaction can function as an acoustic cladding layer, allowing ultrasound to be coupled into an optical fiber and transported over long distances for applications in structural monitoring. While ultrasound testing is widely used today for structural monitoring, the leakage of acoustic energy into the environment prevents it from being transported at significant distances. While it is possible to directly exact a burst into the structure, a pitch-catch or pulse-echo signal quickly becomes extremely complex and difficult to draw meaningful conclusions from.

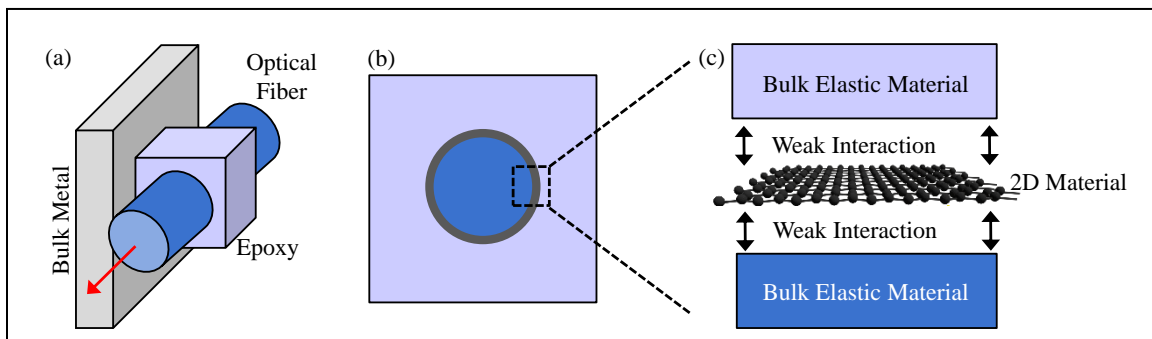


Figure 14. Concept of acoustic guiding with a solid fiber. (a) The continuum view is a thin plate coupled to an elastic half-space with springs. (b) The atomistic view is atoms bounded by many-body and LJ potentials.

The second two objectives involve two extensions of the current work. The first is to extend it to higher frequencies, and the second is to use wave motion as a means of tuning electrical or optical properties. The applicability of continuum models to 2D materials is an active area of

research^{29,30}. This field of research is mostly focused on understanding the elastic properties of 2D materials. However, the next step in this progression, which this thesis focused on, is understanding wave motion in 2D materials (which is a product of their elastic properties). While this thesis focused on wave motion in the ultrasound range for applications in sound isolation or guiding, new knowledge on these wave motions can be extended to higher frequencies, such as those approaching the THz range of optical communication. Here, the acoustic properties of these materials/interfaces can play an important role in timekeeping and interactions with the electromagnetic spectrum. For example, acoustic cavities with 2D materials have already begun to approach resonances in the THz range when using the absorption of ultrafast laser pulses to generate wave motion³¹. The second extension views move the motion as a means of manipulating electrical and/or optical properties of 2D materials, **Figure 15**.

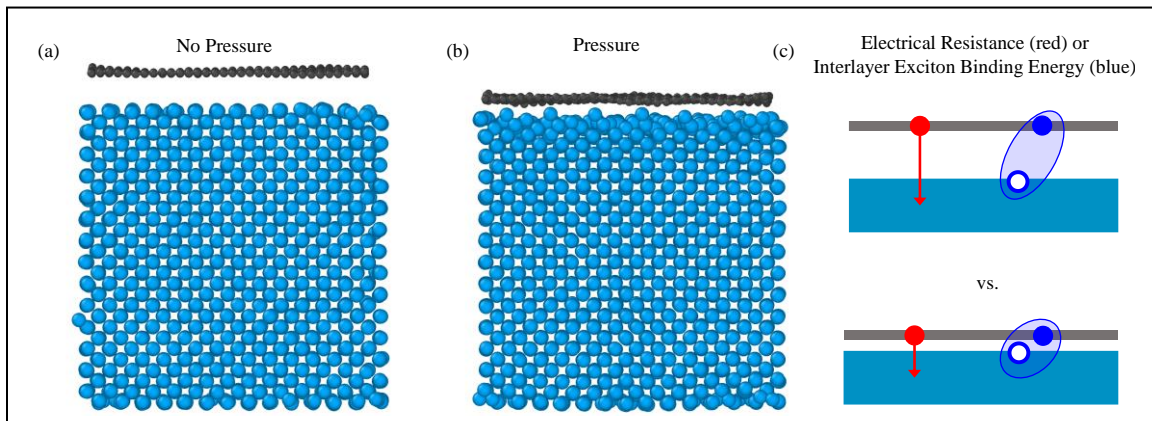


Figure 15. Illustration of wave motion modifying interlayer phenomena in vdW heterostructures. (a) MD simulation showing the vdW separation with no external pressure. (b) MD simulation is showing the same vdW separation with external pressure. (c) Illustration of interlayer electrical and optical phenomena that are sensitive to the vdW separation.

For example, how atomic motions from an acoustic resonance or incoming acoustic pressure can modify these properties. One possible application is to investigate wave motion in vdW heterostructures, which are synthetically layered stacks of arbitrary 2D materials³². In vdW heterostructures, there are numerous electrical and optical interactions that occur between layers. For example, interlayer charge transport or the formation of interlayer excitons^{19,33}. All of these

interlayer phenomena are extremely sensitive to the vdW separation. In fact, interlayer excitons are found to entirely vanish when the vdW separation is even slightly modified¹⁹. Taking note of the changes to the vdW separation under acoustic pressure, Figure 6, it is possible that wave motion may also modulate these interlayer phenomena in to provide new sensors or electrical/optical readouts.

REFERENCES

1. S. Sze and K. Ng. *The Physics of Semiconductor Devices*. John Wiley & Sons (2007)
2. C. Choy. The thermal conductivity of polymers. *Polymer* **18**, 984-1004 (1977)
3. A. Ward, D. Briodo, D. Stewart, and G. Deinzer. Ab initio theory of lattice thermal conductivity in diamond. *Physical Review B* **80**, 125203 (2009).
4. Swartz, E. T. Thermal boundary resistance. *Rev. Mod. Phys.* **61**, (1989).
5. Chiritescu, C., Cahill, D. G., Nguyen, N., Johnson, D., Bodapati, A., Keblinski, P. & Zschack, P. Ultralow thermal conductivity in disordered, layered WSe₂ crystals. *Science* (1979) **315**, 351–353 (2007).
6. Martin, P., Aksamija, Z., Pop, E. & Ravaioli, U. Impact of phonon-surface roughness scattering on thermal conductivity of thin Si nanowires. *Physical Review Letters* **102**, 1–4 (2009).
7. Cummer, S. A. & Christensen, J. Controlling sound with acoustic metamaterials. *Nature Review Materials* (2016). doi:10.1038/natrevmats.2016.1
8. Maldovan, M. Sound and heat revolutions in phononics. *Nature* **503**, 209–217 (2013)
9. Graff, K. *Wave motion in elastic solids*. (Oxford University Press, 1975).
10. Kino, G. *Acoustic Waves: Devices, Imaging, and Analog Signal Processing*. (Prentice-Hall, 1987).
11. Zalalutdinov, M. K., Robinson, J. T., Fonseca, J. J., LaGasse, S. W., Pandey, T., Lindsay, L. R., Reinecke, T. L., Photiadis, D. M., Culbertson, J. C., Cress, C. D. & Houston, B. H. Acoustic cavities in 2D heterostructures. *Nature Communications* **12**, (2021).

12. Brenner, K., Ergun, A. S., Firouzi, K., Rasmussen, M. F., Stedman, Q. & Khruyi-Yakub, Pi. Advances in Capacitive Micromachined Ultrasonic Transducers. *Micromachines (Basel)* **10**, 152 (2019).
13. Novoselov, K. S., Jiang, D., Schedin, F., Booth, T. J., Khotkevich, V. v., Morozov, S. v. & Geim, A. K. Two-dimensional atomic crystals. *Proceedings of the National Academy of Sciences* **102**, 10451–10453 (2005).
14. Schabel, M. C. & Martins, J. L. Energetics of interplanar binding in graphite. *Physical Review B* **46**, 7185–7188 (1992).
15. Persson, B. N. J., Volokitin, A. I. & Ueba, H. Phononic heat transfer across an interface: Thermal boundary resistance. *Journal of Physics Condensed Matter* **23**, (2011).
16. Ong, Z. Y., Cai, Y. & Zhang, G. Theory of substrate-directed heat dissipation for single-layer graphene and other two-dimensional crystals. *Physical Review B* **94**, 1–11 (2016).
17. Ong, Z. Y., Qiu, B., Xu, S., Ruan, X. & Pop, E. Flexural resonance mechanism of thermal transport across graphene-SiO₂ interfaces. *Journal of Applied Physics* **123**, 115107 (2018).
18. Rappe, A., Casewit, C., Colwell, K., Goddard, W. & Skiff, W. UFF, a full periodic table force field for molecular mechanics and molecular dynamics simulations. *J Am Chem Soc* **114**, 10024–10035 (1992).
19. Nayak, P., Horbatenko, Y., Anh, S., Kim, G., Lee, J. U., Ma, K., Jang, A., Lim, H., Kim, D., Ryu, S., Cheong, H., Park, H. & Shin, H. S. Probing evolution of twist-angle-dependent interlayer excitons in MoSe₂/WSe₂ van der Waals heterostructures. *ACS Nano* **11**, 4041–4050 (2017).
20. Bae, S., Kum, H., Kong, W., Kim, Y., Choi, C., Lee, B., Lin, P., Park, Y. & Kim, J. Integration of bulk materials with two-dimensional materials for physical coupling and applications. *Nature Materials* **18**, 550–560 (2019).
21. Suryavanshi, S., Gabourie, A. J., Barati Farimani, A. & Pop, E. Thermal boundary conductance of two-dimensional MoS₂ interfaces. *Journal of Applied Physics* **126**, (2019).

22. Thompson, A., Aktulga, H., Berger, R., Bolintineanu, D., Brown, W., Crozier, P., Veld, P., Kohlmeyer, A., Moore, S., Nguyen, T., Shan, R., Stevens, M., Tranchida, J., Trott, C., & Plimpton, S. LAMMPS - a flexible simulation tool for particle-based materials modeling at the atomic, meso, and continuum scales. *Computer Physics Communications* **271**, 108171 (2022).
23. Lindsay, L. & Briodo, D. Optimized Tersoff and Brenner empirical potential parameters for lattice dynamics and phonon thermal transport in carbon nanotubes and graphene. *Physical Review B* **81**, 205441 (2010).
24. Evans, D. & Holian, B. The Nose-Hoover thermostat. *Journal of Chemical Physics* **83**, 4069 (1985).
25. Tersoff, J. Empirical interatomic potential for silicon with improved elastic properties. *Physical Review B* **38**, 14 (1988).
26. Li, X., Cai, W., An, J., Kim, S., Nah, J., Yang, D., Piner, R., Velamakanni, A., Jung, I., Tutuc, E., Banerjee, S., Colombo, L. and Ruoff, R. Large-area synthesis of high-quality and uniform graphene films on copper foils. *Science* **324**, 5932, 1312–1314 (2009).
27. Suk, J. W., Kitt, A., Magnuson, C. W., Hao, Y., Ahmed, S., An, J., Swan, A. K., Goldberg, B. B. & Ruoff, R. S. Transfer of CVD-grown monolayer graphene onto arbitrary substrates. *ACS Nano* **5**, 6916–6924 (2011).
28. Ferrari, A.C., Meyer, J.C., Scardaci, V., Casiraghi, C., Lasserri, M., Mauri, F., Piscanec, S., Jiang, D., Novoselov, K.S., Roth, S., Geim, A.K. Raman Spectrum of Graphene and Graphene Layers. *Physical Review Letters* **97**, 187401 (2006).
29. Zhang, D. & Dumitric T. Bending ultrathin graphene at the margins of continuum mechanics. *Physical Review Letters* **106**, 25 (2011).
30. Wei, Y., Wang, B., Wu, J., Yang, R. and Dunn, M. L. Bending rigidity and Gaussian bending stiffness of single-layered graphene. *Nano Lett.* **13**, 26–30 (2013).
31. Zalalutdinov, M., Robinson, J., Fonseca, J., LaGasse, S., Pandey, T., Lindsay, L., Reinecke, T., Photiadis, D., Culbertson, J., Cress, C. & Houston, B. Acoustic cavities in 2D heterostructures. *Nature Communications* **12**, 1 (2021).

32. Geim, A. Van der Waals heterostructures. *Nature* **499**, 7459 (2013).
33. Chiu, M., Zhang, W., Hus, W., Terrones, M., Terrones, H., Li, L. Spectroscopic signatures for interlayer coupling in MoS₂-WSe₂ van der Waals stacking. *ACS Nano* **8**, 9649-9656 (2014).